An Improved Vaseline Gap Voltage Clamp for Skeletal Muscle Fibers

BERTIL HILLE and DONALD T. CAMPBELL

From the Department of Physiology and Biophysics, University of Washington School of Medicine, Seattle, Washington 98195. Dr. Campbell's present address is the Department of Physiology, Yale University School of Medicine, New Haven, Connecticut 06510.

ABSTRACT A Vaseline gap potentiometric recording and voltage clamp method is developed for frog skeletal muscle fibers. The method is based on the Frankenhaeuser-Dodge voltage clamp for myelinated nerve with modifications to improve the frequency response, to compensate for external series resistance, and to compensate for the complex impedance of the current-passing pathway. Fragments of single muscle fibers are plucked from the semitendinosus muscle and mounted while depolarized by a solution like CsF. After Vaseline seals are formed between fluid pools, the fiber ends are cut once again, the central region is rinsed with Ringer solution, and the feedback amplifiers are turned on. Errors in the potential and current records are assessed by direct measurements with microelectrodes. The passive properties of the preparation are simulated by the "disk" equivalent circuit for the transverse tubular system and the derived parameters are similar to previous measurements with microelectrodes. Action potentials at 5°C are long because of the absence of delayed rectification. Their shape is approximately simulated by solving the disk model with sodium permeability in the surface and tubular membranes. Voltage clamp currents consist primarily of capacity currents and sodium currents. The peak inward sodium current density at 5°C is 3.7 mA/cm^2. At 5°C the sodium currents are smoothly graded with increasing depolarization and free of notches suggesting good control of the surface membrane. At higher temperatures a small, late extra inward current appears for small depolarizations that has the properties expected for excitation in the transverse tubular system. Comparison of recorded currents with simulations shows that while the transverse tubular system has regenerative sodium currents, they are too small to make important errors in the total current recorded at the surface under voltage clamp at low temperature. The tubules are definitely not under voltage clamp control.

INTRODUCTION

This paper describes a potential recording and voltage clamp method rapid enough to give good control of transient sodium currents in frog skeletal muscle fibers. Previous work has already led to four technically different approaches to this problem: two- and three-microelectrode clamps (Kao and Stanfield, 1968; Adrian et al., 1970 *a*), double sucrose gap clamps (Ildefonse and Rougier, 1972; Nakajima and Bastian, 1974), internal axial wire clamps (Davies, 1974), and triple Vaseline gap clamps with potentiometric recording (Frankenhaeuser et al., 1966;

Moore, 1972). Our method is a potentiometric Vaseline gap method, very similar to its predecessors, but with numerous small changes making it significantly more faithful as a voltage clamp. The method is described here. The following two papers concern the ionic selectivity, kinetic properties, and some pharmacological properties of sodium channels in muscle.

METHODS

Problems

The reader is referred to the original papers from Frankenhaeuser's laboratory for an introduction to the principles of his potentiometric method. Frankenhaeuser (1957) developed the fast potentiometric recording technique for single myelinated nerve fibers using a chamber with four compartments, three Vaseline seals, and one feedback amplifier. Dodge and Frankenhaeuser (1958) added a second feedback amplifier to obtain a voltage clamp. The arrangement of electrodes around the fiber and the feedback circuit were in most respects like those of Fig. 1. When they applied this technique without further modification to single muscle fibers, Frankenhaeuser et al. (1966) noted advantages of longevity and ability to polarize the membrane potential away from rest compared with microelectrode work. There were still, however, severe electrical disadvantages compared with the results on myelinated fibers. They found a large DC error in attempts to measure absolute membrane potential and a significant dynamic error in measurements of voltage changes. Current could easily be applied to the fiber but its magnitude and time-course could not be determined. Finally the dissection of single muscle fibers is more tedious than the dissection of a single myelinated nerve fiber. We have identified and corrected sources of many of these difficulties.

Preparation

Fibers are dissected from the semitendinosus muscles of very large (8–11 cm) specimens of the frog *Rana pipiens*. The muscle is mounted in a dissection dish under Ringer solution and the ventral head cut away. Then half the dorsal head is also cut away lengthwise leaving the remaining fibers in a thin layer. Fibers are not dissected from end to end. Instead, watchmaker's forceps are used to pinch off and pull away approximately 10-mm lengths of one or several fibers from the edge of the muscle. If several fibers are taken, single fibers are then peeled apart with forceps. Fibers are plucked off the edge of the muscle until one with a diameter of 80–130 μm and an undamaged length of about 6 mm is obtained. Only fibers that twitch when pinched by the forceps are used. The selected piece of fiber is transferred quickly with forceps to the acrylic chamber containing a depolarizing solution like 120 mM CsF covering all pools and partitions. The fiber shortens and typically attains a major diameter of 150–180 μm. Seventeen measurements on six such fibers in CsF gave a sarcomere length of 1.6 ± 0.2 μm (mean ± SD). This highly simplified dissection has the advantages of taking only a few minutes and of permitting many fibers to be prepared from one muscle.

The recording chamber with three partitions and four pools is the same as those used in our studies of myelinated nerve (Hille, 1971). Throughout these papers we use the notations given in Fig. 1, e.g., pools A, B, C, and E, point D, amplifiers A1, A2, etc. In addition the voltages appearing at A, C, D, and E are referred to as V_A, V_C, V_D, and V_E. Typical dimensions of the chamber (in micrometers) are: BC partition, 500; B pool, 250; AB partition, 200; A pool, 80–150; and EA partition, 200.

The shortened muscle fiber fragment is mounted by positioning the undamaged region across the three partitions that have previously been covered with strings of

Vaseline. Three Vaseline seals are then applied over the fiber and both ends of the fiber are cut once again, this time with fine scissors, leaving an attached stump of only 300–500 μm in the E pool and of ca. 250 μm in the C pool. This second cut, done within 5 min after the fiber is obtained, removes the damaged ends of the fiber fragment and also a considerable length of apparently healthy material. The new cut end remains square and healthy looking without any clotting or shrinkage through the rest of the experiment.

The fluid level is lowered until all compartments become electrically isolated, and finally the solution in pool A only is replaced by Ringer. The standard frog Ringer solutions used in this paper contains 115 mM NaCl, 2 mM KCl, 2 mM $CaCl_2$, 4 mM tris(hydroxymethyl)aminomethane-HCl buffer, pH = 7.4. Pools B, C, and E remain filled with CsF throughout the experiment. One reason for depolarizing the fiber before applying seals is that the transient contracture upon applying depolarizing solution can dislodge seals. Efforts to stretch fiber fragments to more normal sarcomere lengths before applying seals led to problems as the fiber slowly shortened again over the next 30 min.

The procedure described so far has several advantages over the previous method (Frankenhaeuser et al., 1966; Moore, 1972). Cutting the fiber ends lowers the impedances Z_{DC} and Z_{ED} from the inside of the artificial "node" in A to the recording pool C and current-delivering pool E possibly fourfold. This significantly increases the fidelity of the signal reaching amplifier A1 and reduces the gain needed in A2 to achieve good voltage clamp control of the fiber. The new impedance Z_{ED} is not only smaller but has much simpler AC properties, making it possible, as is shown later, to record the membrane current more faithfully. The use of larger fibers and a narrower A pool than before decreases spatial nonuniformities of potential inside the fiber in A. Fluoride-containing solutions in the end pools help to keep the ionized calcium activity low in the myoplasm. With a solubility product of 3.4×10^{-11} M^3 at 18°C for CaF_2, the free calcium is 2.4×10^{-9} M in solutions containing 120 mM free F^-. These fluoride-treated fibers show no contraction when the membrane in pool A is subsequently depolarized by applied current pulses. Placing the depolarizing solution in the B pool as well as the C pool is an essential improvement that eliminates a large demarcation current that prevented Frankenhaeuser et al. (1966) from measuring absolute membrane potentials. Moore (1972) also used a depolarizing solution in pool B but then surrounded the entire fiber in pool B with Vaseline. We did not attempt to place Vaseline in pool B. Frankenhaeuser et al. (1966) observed large potential deviations inside the fiber during excitation, a dynamic error they attributed to unwanted membrane activity under the Vaseline seals. We did not encounter this problem with depolarizing solutions in E, B, and C perhaps because most of the fluid under the seals was not suitable for maintaining excitability.

Control Circuit

The principles of the voltage clamp circuit shown in Fig. 1 are the same as those of the original Dodge-Frankenhaeuser (1958) method. Amplifier A1 keeps point D and pool C at virtual ground to achieve the potentiometric recording condition. Ideally with A1 operating and correctly balanced, no current flows down the fiber to the left of point D. In practice we assume that the resting potential of the muscle membrane is −90 mV and simply adjust the DC balance of A1 until the potential in the A pool is 90 mV. Therefore we have not actually measured the zero current potential in these experiments. When voltages are applied to the E pool, current flows via the impedance Z_{ED} across the muscle membrane in the A pool. If the voltage in E is applied from a waveform generator we say the fiber is under "current clamp" although no feedback is applied to hold the current to the desired waveform. Voltage clamp is achieved by switching in the voltage control

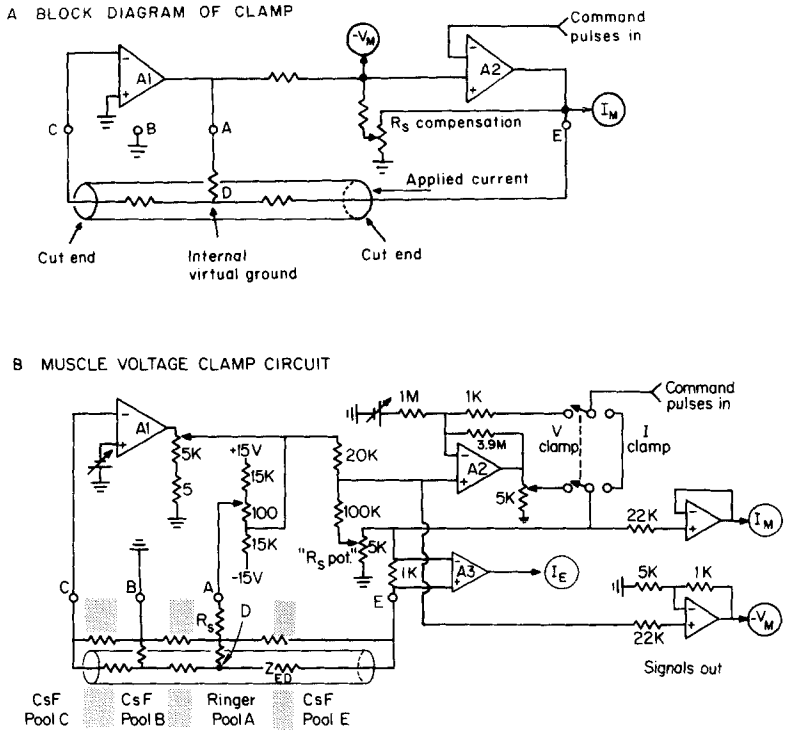
A BLOCK DIAGRAM OF CLAMP
Command pulses in
A1
A2
$-V_M$
I_M
C
B
A
D
E
R_S compensation
Applied current
Cut end
Internal virtual ground
Cut end
B MUSCLE VOLTAGE CLAMP CIRCUIT
Command pulses in
1M
1K
3.9M
V clamp
I clamp
A1
A2
A3
5K
+15V
15K
5
100
15K
-15V
20K
100K
"R_S pot."
5K
1K
22K
I_E
$-V_M$
R_S
Z_{ED}
Signals out
CsF Pool C
CsF Pool B
Ringer Pool A
CsF Pool E
C FREQUENCY RESPONSE OF FEEDBACK AMPLIFIERS
Gain
1,000
400
200
100
40
20
10
A1
A2
Measured with 50-Ω source impedance
10
100
1K
10K
100K
1M
Frequency (Hz)

FIGURE 1.

amplifier A2. It applies membrane current, again through Z_{ED}, to keep $-V_M$ equal to the command pulses.

As in Nonner's (1969) method and in our standard method (Hille, 1971) for myelinated fibers, we have used single electrodes to connect to pools A, B, and E rather than the pairs used by Dodge and Frankenhaeuser (1958). We later discovered that with the 100-fold lower impedances of muscle preparations relative to myelinated nerve fibers, the external fluid resistance R_s in the A pool leads to a significant error in membrane potential during current flow. Therefore if the apparatus were built again we would prefer to include a separate potential-measuring electrode in A. We estimate that reverting to two electrodes in A and making no effort to bring the recording electrode very close to the fiber might reduce the series resistance problem by 30–50%. Instead we added electronic compensation for the effective external series resistance R_s. A variable fraction of the current signal selected at the "R_s potentiometer" (Fig. 1 B) is summed with the potential signal to reconstruct the potential on the muscle side of R_s, as has been done in other systems (Hodgkin et al., 1952). The method for setting the potentiometer is described later. The "corrected" potential is also brought out to the oscilloscope as the signal labeled $-V_M$. This feature allows the effects of the correction to be observed even under current clamp where there is no danger of positive feedback from overcompensation.

Nonner (1969) has given an excellent illustration of how, with knowledge of phase lags and leads in the preparation, the voltage clamp amplifier can be tailored to extend its useful gain to very high frequencies. In particular the often used method of limiting the high frequency response of a good amplifier by a single time constant roll-off severe enough to eliminate oscillations in the voltage clamp probably makes the least use of the possibilities of the amplifier. This is because most kinds of preparations have input-output relations with phase lags exceeding 90° at frequencies well within the range of physiological importance. Adding to this an amplifier introducing 90° of additional phase lag at the same frequencies would necessarily give oscillations as the gain is increased. When the amplifiers used in our myelinated nerve work were applied to muscle, turning

FIGURE 1. Simplified circuit of voltage clamp and current clamp and frequency-gain characteristics of amplifiers. (A) Block diagram of voltage clamp. Amplifier A1 keeps the inside of the fiber at virtual ground for potentiometric recording of membrane voltage. A2 is the voltage clamp amplifier. (B) Equivalent circuit of preparation showing four fluid-filled pools connected via electrodes (circles) to control circuit. Capacitance and electrogenic properties of the muscle fiber are not represented. Stippled areas represent Vaseline-covered partitions separating the fluid pools. Amplifiers A1, A2, and A3 are differential, high input impedance amplifiers with gain of ×1,000 at low frequencies and high frequency characteristics as shown in part B. The other two amplifiers are conventional operational amplifiers. The variable DC potential source at the input of A1 makes up for junction potentials and offsets in the C pool and its calomel electrode. The variable DC potential source in series with the A electrode offsets the resting or holding potential to keep the output of A1 and the input of A2 near ground (Nonner, 1969). (C) Bode plot of the frequency response of amplifiers A1 and A2. Dashed line shows the slope of a one-time constant roll-off. Amplifier A3 has a roll-off of this slope starting at 25 kHz. The responses are shaped by feedback elements within the amplifiers that do not compromise the differential input impedance of the amplifiers. In each amplifier the input includes a dual FET transistor AD3954A (Analog Devices, Inc., Norwood, Mass.).

up the gain of amplifier A1 gave oscillations in the range of 2–5 MHz and amplifier A2 gave "ringing" in the range 5–10 kHz. Therefore, the different phase characteristics of the muscle preparation were measured roughly and the frequency responses of the amplifiers were altered by using internal feedback elements with numerous fixed capacitors and resistors. Both amplifiers A1 and A2 are based on a discrete design by D. Weymann kindly described to us by Drs. W. Nonner and R. Stämpfli. The available high frequency gain is higher than in ordinary commercial operational amplifiers. The open-loop frequency response of each amplifier after trimming with the chosen internal networks is given in Fig. 1 C. The significant point is that the frequency response is either flat or falling with only a very shallow slope to keep phase lags well below 90° at all frequencies of physiological interest. As indicated in the circuit of Fig. 1 B, there are no capacitors outside of the amplifiers in the voltage clamp circuit to limit the frequency response of the system. Of course the preparation itself has stray and membrane capacitative elements.

Leak Subtraction

To study the properties of one ionic channel under voltage clamp, methods must be found to block or subtract currents in other channels and to substract capacity currents. In muscle fibers cut in CsF both the delayed rectifying and the inwardly rectifying potassium channels seem to be inoperative. Further treatment of fibers with high external concentrations of tetrodotoxin blocks sodium channels, leaving membrane currents that are nearly perfectly symmetrical for positive and negative voltage steps. This linear capacity transient and "leakage current" can readily be subtracted automatically from the current record during the experiment as is done in our studies of myelinated nerve (Armstrong and Hille, 1972). The "leak subtractor" circuit in Fig. 2 A sums a step current with three exponentially decaying currents to imitate leakage and a three-time constant capacity transient during step voltage changes. As is shown in Fig. 2 C, the membrane current signal and the output of the leak and capacity circuit are fed into the differential amplifier of the oscilloscope and suitably adjusted to cancel capacity and leakage current from the displayed current record. In practice the adjustment of the capacity subtractor is done with small hyperpolarizing or depolarizing voltage steps. Particularly in muscle where charging of the tubules takes significant time, this capacity subtraction facilitates study of the rapid transient sodium currents from the surface membrane. However, use of the technique in fibers not poisoned with tetrodotoxin inherently assumes that the charging transient of tubules remains symmetrical even though there are active sodium channels in the tubules. This assumption is definitely wrong, and the inherent error is considered later. The Z_{ED} compensator circuit shown in Fig. 2 B is also discussed later.

RESULTS

The first part of Results consists primarily in electrical tests to ascertain how well the recorded potential and current signals reflect the actual potential and current flowing in the muscle fiber. The errors considered include *(a)* deviation of the internal potential V_D through imperfect operation of the feedback loop containing amplifier A1, *(b)* deviation of the internal and external potentials from their expected values due to local IR drops of currents flowing to the membrane, and *(c)* distortion of the current record by the impedance of the end of the fiber through which the current is delivered.

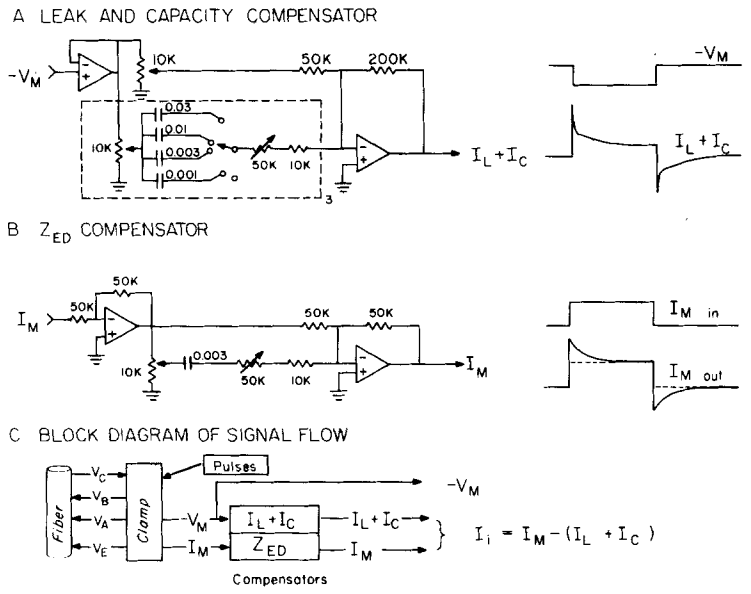

FIGURE 2. Simplified circuit diagrams of compensating and correcting circuits for record and block diagram of signal flow. The leak and capacity circuit and the Z_{ED} compensating circuit are basically similar and sum a fraction of an incoming signal with selected high frequency components of the signal giving the waveforms shown at the right. The part of circuit in A surrounded by a dashed box is repeated three times to produce three independent time constants in response to a step input. The position of the compensating circuits in the signal pathway is shown in C. The parts labeled fiber and clamp are detailed in Fig. 1 B.

Potential Record with no Membrane Current

In the Frankenhaeuser (1957) potentiometric recording method, the inside of the fiber (point D) is supposed to be held at virtual ground by negative feedback from the first amplifier A1 (see Fig. 1 A). With the inside at ground, the membrane potential E_M of the segment of fiber in pool A can be measured simply by recording the potential V_A in the A pool, but with a minus sign to conform with the usual inside-minus-outside convention. However, the identification of $-V_A$ with E_M is incorrect if D deviates from ground, which can happen if the feedback amplifier A1 has too little gain, if the error signal from point D is too severely attenuated before reaching the amplifier at pool C, or if currents from electrical activity under seals BC or AB or in pools B or C are added to the error signal. These errors were investigated by recording the potential at D with a glass micropipette electrode as described in the next paragraph. The fibers were easy to impale in the chamber and gave stable records for up to an hour.

The six frames in Fig. 3 show simultaneous recordings of the potential V_D on a microelectrode at point D and the inverted potential on the A calomel electrode ($-V_A$). The sum of the traces in each case is the membrane potential E_M. Capacity neutralization of the microelectrode amplifier is adjusted to square up

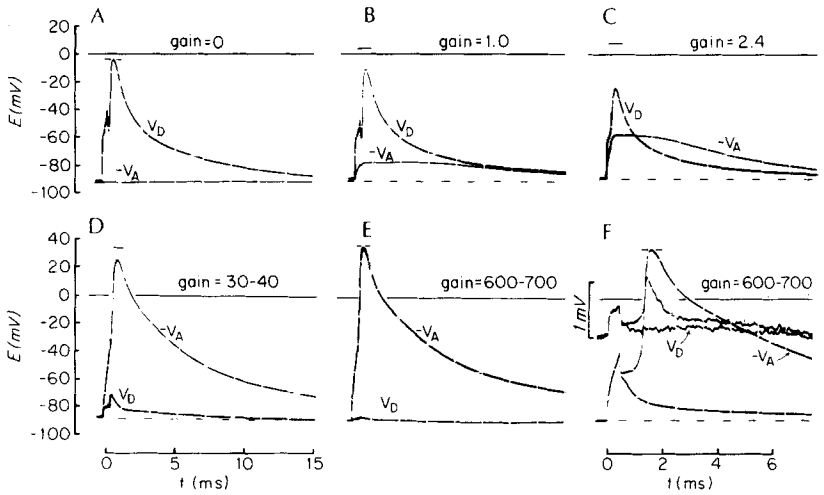

FIGURE 3. Test of the control of V_D by amplifier A1. The fiber is impaled by a 5-MΩ recording microelectrode in pool A. The internal signal recorded with a capacity-neutralized follower is V_D and the inverted external signal in A is $-V_A$. The V_D trace has been lowered by 90 mV for the illustration and is more properly a positive signal starting with a base line at 0 mV. The switch in Fig. 1 B is in the "I clamp" position. In A, amplifier A1 is off entirely. In the successive frames, A1 is connected and its effective gain gradually increased to the values given by adjusting the 5-kΩ potentiometer at its output. The values given are the low frequency gain. Frame F has a different time scale and the gain on V_D is much higher. The maximum rate of rise of the action potential was 200 V/s. The fiber was cut in 80 mM K_2SO_4. Temperature 18°C.

the response to square currents injected through a tiny capacitor at the input while the electrode is just outside the fiber in pool A. Action potentials are elicited by short pulses applied to the E pool. In successive frames the feedback applied from C to A is gradually increased by turning up the 5-kΩ potentiometer at the output of A1 to achieve control of V_D. The stimulus voltage in pool E is also reduced in each successive frame. With no feedback (DC gain = 0), V_D shows a membrane action potential and $-V_A$ is steady at −90 mV. The action potential is small and short since the active membrane in pool A is electrically loaded by low impedance connections to pools E and B. As the feedback gain is increased, the signal at V_D is reduced and $-V_A$ takes on the shape of the action potential. Summing the signals to calculate E_M shows that the action potential peak (marked by horizontal bars) and the duration both increase as the loading effect of E and B is removed by feedback. In the last frame the small dynamic error remaining in V_D is seen to be less than 1 mV, showing that $-V_A$ faithfully portrays the full membrane potential change. For comparison Frankenhaeuser et al. (1966) show a 50-mV negative change in V_D during the stimulus and a 10-mV positive change near the peak of the action potential. Three factors may contribute to the improvement here. Cutting the fiber in pool C improves the transmission of the error signal to pool C. Replacing the Ringer in pools B and C

reduces contributions from excitability outside the A pool. Finally our amplifier A1 may have had more high frequency gain than that used by Frankenhaeuser et al.

Quantitative comparison of $-V_A$ and V_D in Fig. 3 indicates that low frequency signals at V_D are transmitted to the input of amplifier A1 in pool C with very little decrement, unlike the situation with myelinated nerve. Between 80 and 90% of V_D is recorded at pool C. This is determined by noting that for waveforms as slow as the falling phase of the action potential, $-V_A$ is about 0.8–0.9 times the product of the amplifier gain times V_D in each of the frames of Fig. 3. An obvious exception occurs when the amplifier is driven to saturation by signals exceeding ± 13 mV at the input, as is seen from the flattening of $-V_A$ during the action potential in frames B and C of Fig. 3. For faster waveforms like those of the rising phase of the action potential, the "error signal" V_D is not as effectively amplified by A1 (see $-V_A$ in frames D and F) probably because of some attenuation before the signal reaches the amplifier input in C and also because the amplifier has less gain at high frequencies (see Bode plot in Fig. 1 C).

The good transmission of low frequency signals from D to C means that the seal resistance R_{BC} is much higher than the myoplasmic resistance R_{DC}. The resistance to ground through the membrane in the B pool must also be higher than R_{DC}. Geometrical considerations suggest that R_{DC} is 100–150 kΩ in a 140-μm diameter muscle fiber or possibly two orders of magnitude lower than in a large myelinated nerve fiber. All of these factors in muscle mean that small errors in junction potentials and amplifier unbalance will give only small DC offsets in V_D and hence equally small errors in the externally measured membrane potential. In the node of Ranvier the potential V_D has never been measured, but there are reasons to suppose that it may be mistakenly held 10–15 mV off of ground in many experiments. By contrast, in the experiment of Fig. 3, the potential change recorded on transferring the microelectrode from point D to the grounded B pool was less than 3 mV. In the node of Ranvier, recorded potential changes are thought to be less than the full value because of an "attenuation artifact" (see Dodge and Frankenhaeuser, 1958, 1959). In the simplest case, this artifact would show up during action potentials as a positive-going deflection of V_D with a shape exactly similar to the time-course of $-V_A$. Any such effect is so small in frame F of Fig. 3 as to be negligible. In conclusion, the favorable impedances of the muscle preparation allow membrane potentials to be recorded potentiometrically with little offset, dynamic error, or attenuation artifact when the density of membrane current is low.

Intracellular Potential with Membrane Current Flowing

When the membrane current density becomes appreciable, two more errors appear in the potential record arising from new potential drops in fluid resistances of the preparation. One is the well-known extracellular potential drop between the recording point on calomel electrode A and the fiber surface in pool A. The other is the intracellular longitudinal potential drop across the width of the artificial node in pool A leading to deviation from the "space clamp" condition. Both errors can be understood by relatively simple models and both

may be measured with a glass microelectrode. The space clamp problem is considered first.

The magnitude of the intracellular potential drop within the artificial node may be estimated by a simple first-order theory based on linear one-dimensional cable theory. Making reference to Fig. 1 B, take x as the distance coordinate with $x = 0$ at the AB seal. Call the width of the A pool l, the intracellular specific resistance R_i, the membrane current density I_M, and the fiber radius a. We calculate the intracellular potential profile $V_D(x)$ by making the approximation that the potential deviations are too small to affect the current density in any patch of membrane. This approximation holds to any desired accuracy for linear and nonlinear cases provided the potential deviations are small enough. Then from cable theory

$$\frac{d^2V_D}{dx^2} = \frac{2R_iI_M}{a}. \tag{1}$$

Integrating with I_M constant and noting that the point at $x = 0$ is still maintained at a virtual ground by feedback from amplifier A1 gives

$$V_D(x) = R_iI_Mx^2/a. \tag{2}$$

And finally the extreme deviation at $x = l$ is

$$V_D(l) = R_iI_Ml^2/a \tag{3}$$

From the area under a parabola, the mean voltage deviation over the entire node is one-third of the value $V_D(l)$.

For a given fiber radius the error goes up as l^2, and for fibers of different radius mounted in chambers with a constant l/a ratio, the error increases as the radius. Moore et al. (1975 *a*, *b*) have calculated $V_D(x)$ for nearly the same problem, an axon in a double sucrose gap, again using one-dimensional cable theory but solving the Hodgkin-Huxley equations explicitly at each membrane patch. The values of $V_D(l)$ calculated by our simple formula agrees well with those obtained by Moore et al. in each of their numerical examples, showing that for small voltage deviations (<15 mV) the assumption of constant current density over the entire nodal membrane is adequate for order of magnitude calculations of the voltage error. A footnote and some of the discussion in Moore et al. (1975 *b*) leave the incorrect impression that deviations of V_D might be proportional to the ratios l/a or $l/\sqrt{a}$ instead of l^2/a. For example it is stated that errors are small provided the artificial node is shorter than the axon diameter. A simple way to explain the l^2/a factor is to note that the error is proportional to the total membrane current through the node times the total longitudinal resistance of the node. The first factor varies as la and the second as l/a^2.

To calculate $V_D(l)$ it is not necessary to determine R_i, I_m, and a if the more readily measured potential V_E in the E pool and length k of the fiber segment from $x = l$ to the cut end in pool E are known. The axial resistance R_{ED} of this fiber segment is $R_ik/\pi a^2$ and the axial current is $2\pi alI_m$. If all the current enters through the cut end, the potential drop in the fiber segment is $2klI_MR_i/a$. Adding this to $V_D(l)$ (Eq. 3) gives V_E, and solving for V_D

$$V_D(l) = V_El/(l + 2k). \tag{4}$$

Typical values of l and k in our experiments are 100 and 700 μm making the estimated $V_D(l)$ equal to $V_E/15$.

The estimate of V_D errors may be compared with micropipette recordings. The time-courses of V_E and of V_D near the AE seal are shown in Fig. 4 for a fiber under voltage clamp. The three superimposed sweeps show the responses to no pulse, to a modest depolarizing pulse giving maximum inward sodium current, and to a large depolarization beyond the sodium reversal potential. As expected, the time-courses of V_D and V_E are similar, and V_D is 25 times smaller than V_E. The peak voltage deviation near $x = l$ is 5 mV in this fiber, and therefore the mean of the peak value over the whole node is 1.7 mV. Reimpaling the fiber near the AB seal showed deviations of V_D well under 1 mV at the end of the clamped fiber. This kind of experiment was repeated on six fibers with similar results. We also verified that the errors become much more severe when the A pool is deliberately made wider.

Our simple formula and the calculations of Moore et al. (1975 *a*, *b*) may be criticized for using one-dimensional cable analysis for cases where the diameter of the cable is comparable to its length. Indeed as the depth of penetration was varied, the signal on the micropipette changed both in magnitude and in the apparent relative contributions of sodium, capacity, and leakage currents to its shape. This variation was not explored systematically but suggests an interesting principle for sorting out the relative contributions of surface membrane and transverse tubular membranes to the total membrane currents: Longitudinal current flowing along the periphery of the fiber should have a time-course closer to that of the surface membrane current while longitudinal current in the center of the fiber should have a time-course closer to that of tubular membrane currents. However a variable leak around the site of membrane penetration might make practical exploitation of this idea difficult.

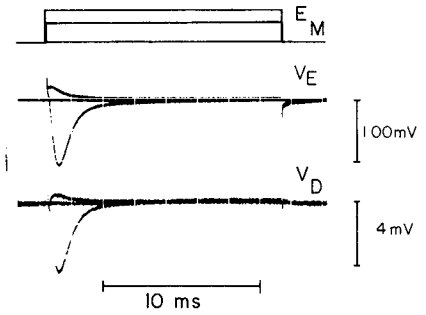

FIGURE 4. Measurement of the internal voltage error due to current flow. The membrane is stepped to voltages on both sides of the sodium reversal potential under voltage clamp and the resulting current signal I_M recorded without corrections for Z_{ED}, leak, or capacity. The fiber is also impaled by a recording microelectrode in the A pool segment, very close to the EA seal. The internal signal V_D recorded with a capacity-neutralized follower shows the extreme value of the internal potential deviation during current flow. The external series resistance compensation was off but turning it on did not change the V_D error signal except insofar as I_M was changed. Width of the A pool 100 μm. R_{ED} = 144 kΩ. Fiber ends cut in 115 mM CsF + 5 mM NaF. Temperature 5°C.

Extracellular Potential during Current Flow

A second source of errors in the membrane potential record is from voltage drops outside the fiber during current flow. The effective external resistance R_s in Fig. 1 A lies primarily in the bathing medium near the fiber and also includes a small contribution from the connecting salt bridge and calomel electrode. Under current clamp the problems of series resistance are seen as instantaneous steps in the potential record V_M when step currents I_M are turned on and off (Fig. 5 A). Under voltage clamp comparable errors in the voltage record may be detected by placing a recording micropipette immediately outside the fiber. Fig. 5 C shows the error voltage ΔV defined as the difference between the micropipette signal and the signal labeled $-V_M$ in Fig. 1. The voltage clamp brings V_M from −90 to −15 mV, but by the peak of the sodium current the actual membrane potential deviates by 20 mV in the positive direction. The ratio of the error ΔV to the voltage V_E in the E pool should be equal to the resistance ratio R_s/R_{ED}. In the fiber of Fig. 5 A the ratio is 0.12 and in the fiber of Fig. 5 C, 0.066. The value of R_{ED} was found to be 97 kΩ in the second fiber making the estimated R_s 6.4 kΩ or, when referred to the surface area of fiber in the A pool, 4.2 Ωcm².

The effects of series resistance may be reduced by electronic compensation.

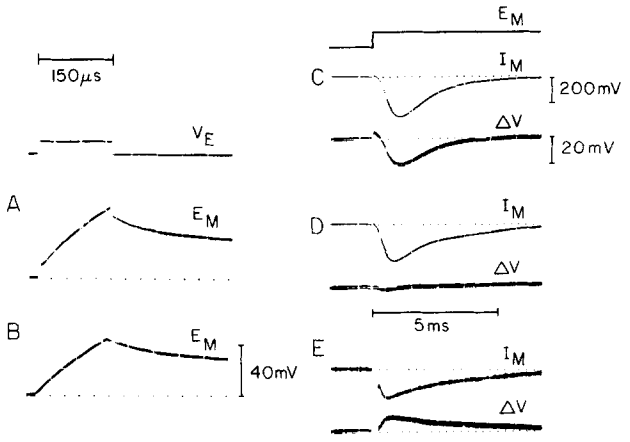

FIGURE 5. Effect of series resistance compensation on the current and voltage records. (A, B) Fiber under current clamp with 40-mV stimulus pulse (V_E) applied in E. (A) Without R_s correction E_M rises first in a step and then with a slower time-course appropriate for charging the membrane. (B) Setting the R_s compensator to 0.12 eliminates the quick step on the record. (C–E) A different fiber under voltage clamp stepped from −90 to −15 mV. The membrane current record I_M is corrected for leak and capacity. The record ΔV is difference between the potential recorded by a microelectrode in pool A immediately outside the fiber and the output signal $-V_M$ from the clamp circuit (Fig. 1 A). Settings of the R_s compensator are 0.0 (C), 0.067 (D), and 0.11 (E), where the system is on the verge of oscillation. Note that the shape of the current record is different in each case. R_{ED} in this fiber was 97.3 kΩ and the membrane area 6.2 × 10^{-4} cm² so 200 mV of I_M signal is equivalent to 3.4 mA/cm² of current. Both fibers are cut in 115 mM CsF + 5 mM NaF. Temperature 5°C.

Turning up the potentiometer labeled "R_s pot." in Fig. 1 B allows compensation of errors up to the equivalent of R_s/R_{ED} values of 0.2. We refer to the maximum setting on the potentiometer as 0.2. Fig. 5 B shows that a setting of 0.12 removes the step from the voltage record in the first fiber under current clamp, and Fig. 5 D shows that a setting 0.07 nulls the error signal ΩV in the second fiber under voltage clamp. Both values are reasonable from the calculations presented. However, in practice the two methods illustrated give different results on the same fiber. In the fiber of Fig. 5 A and B a setting of only 0.100 compensated the measured external ΩV under voltage clamp, and at a setting of 0.105 the system became unstable from positive feedback. In the fiber of Fig. 5 C–E the dial could be turned to 0.11 (Fig. 5 E) under voltage clamp where the system became unstable, but a setting of 0.128 was needed to eliminate the voltage step under current clamp. One important reason for these discrepancies will become clearer later where it is shown that high frequency components of the membrane current are attenuated in the signal I_M used to obtain the compensating waveform. A second less quantitatively significant reason is that the internal current-dependent voltage deviations $V_D(x)$, though small, are in a direction to cancel deviations caused by external series resistance (Ramón et al., 1975). Our inability to find a routine, practical way to determine the correct setting of the compensation dial is unfortunate, since, as is seen in Fig. 5 C–E, the time-course of the sodium current varies significantly with the setting.

In summary three sources of error in the membrane potential record have been examined. Feedback amplifier A1 successfully keeps $V_D(0)$ close to ground potential with only small dynamic errors and DC offset. Current flow causes dynamic deviations from the internal space clamp conditon that can be kept quite small by using a narrow A pool. Current flow causes a large dynamic voltage drop in the extracellular medium, but this error can be compensated electronically. Unfortunately, there is no exact criterion for correct setting of the compensation. We thus have confidence that the membrane potential of the surface membrane of the fiber can be measured with fair fidelity by the potentiometric method. However, as in other known methods, the luminal potential of the transverse tubular system is definitely not held under space clamp so parts of the preparation will not be under voltage clamp control. Errors introduced by the problems of tubular control are considered later.

Fidelity and Corrections of the Current Record

In the Dodge-Frankenhaeuser (1958) potentiometric voltage clamp of nerve, the current is measured as the voltage drop $V_E - V_D$ in the natural impedance Z_{ED} of the preparation. In practice, only the signal V_E is required, as V_D is at ground potential, and with nerve the impedance Z_{ED} is assumed to be a pure and constant resistance R_{ED} at all frequencies. In previous work with an intact end of a muscle fiber in pool E the impedance Z_{ED} was shown to be too complicated by the rectifying and complex capacitative properties of the E pool membrane for this method to be useful (Frankenhaeuser et al., 1966; Moore, 1972). In our preparation CsF stops the membrane rectification, and cutting the fiber vastly extends the frequency range over which Z_{ED} behaves as a simple resistor. Nevertheless the assumption that Z_{ED} is simple at all physiologically interesting

frequencies is poor enough that an independent measure of membrane current is desirable.

As is shown in Fig. 1 B, the absolute current I_E flowing to the E electrode was measured as the voltage drop across a 1-kΩ (sometimes 10 kΩ) resistor by the differential high impedance amplifier A3. The current I_E flows by two pathways towards the A pool and is given by

$$I_E = \frac{V_E - V_D}{Z_{ED}} + \frac{V_E - V_A}{R_{EA}}. \quad (5)$$

The first term in Eq. 5 is the membrane current I_M and the second term is leak through the EA seal. For the moment we consider Z_{ED} to be a simple resistor R_{ED}. With myelinated nerve more current flows through the 2–10-MΩ EA seal than through the 10–30-MΩ axoplasmic resistance R_{ED} so that I_E neither has the time-course nor the amplitude of I_M. However, with a cut muscle fiber, R_{ED} is several orders of magnitude lower than with a myelinated nerve fiber, and the signal I_E more accurately reflects the current flowing down the fiber axis to the membrane under study.

The method for measuring R_{EA} and R_{ED} using Eq. 4 is shown in Fig. 6 A on a preparation with an unusually poor seal. A 56-mV stimulus pulse lasting 0.5 ms is applied to the E electrode giving rise to an action potential (E_M) in the A pool. The current trace I_E is recorded on two superimposed sweeps differing by a factor of 25 in gain. The low gain trace reveals an 800-nA current flowing during the 0.5-ms stimulus indicating that the parallel combination of R_{ED} and R_{EA} provides a 70.0-kΩ pathway from the E pool. The high gain trace reveals current leaking through the EA seal with the time-course of the action potential in the A

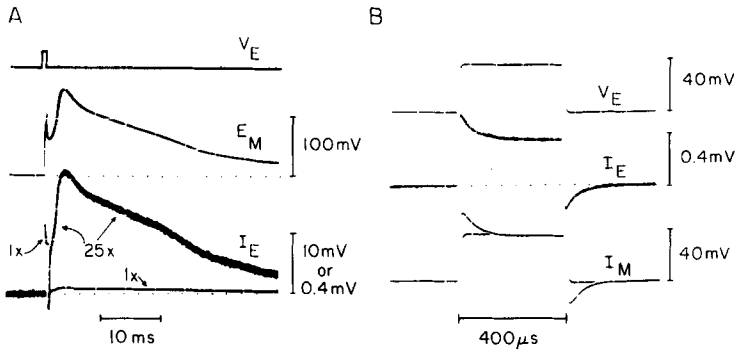

FIGURE 6. Measurement of the impedances R_{EA} and Z_{ED} in current clamp conditions to permit calibration of the current record. (A) A 500-μs 56-mV stimulus pulse (V_E) is applied to the E pool and triggers an action potential (E_M). The current signal (I_E) recorded across a 10-kΩ resistor by amplifier A3 is given at two gains. (B) A 400-μs 35-mV pulse (V_E) is applied to the E pool and the current (I_E) recorded by amplifier A3 across a 1.0-kΩ resistor. The lower trace (I_M) is the output of the Z_{ED} compensating circuit before and after it is adjusted to match the time-course of I_E. The signals V_E I_E, and I_M are all recorded with a single time constant cutoff at 25 kHz. Both fibers are cut in 115 mM CsF + 5 mM NaF. Temperature 5°C.

pool. The 80-nA current at the 145-mV peak of the action potential corresponds to a R_{EA} leak of 1.8 MΩ. Thus in this preparation R_{ED} was 72.8 kΩ and R_{EA} 1.8 MΩ and I_E was very closely equal to the membrane current. In all other preparations where R_{EA} and R_{ED} were measured, their ratio was even larger than the 25:1 value in the example in Fig. 6 A so the leak current proportional to the action potential was barely resolved. From now on we ignore the minor contamination of I_E by seal currents and assume that I_E faithfully represents the magnitude and time-course of membrane current.

Once a reliable method to measure current is available, the nature of the impedance Z_{ED} can be investigated. Fig. 6 B shows how this is done and how the current record I_M can be improved by a first-order correction. The top trace V_E shows a 500-μs 36-mV pulse applied to the E pool. If Z_{ED} were a pure resistor, the current trace would be a similar square pulse, but the measured current I_E shown below actually overshoots. The time-course is roughly explained by a Z_{ED} of 60 kΩ in series with the parallel combination of 52 kΩ and a 2-nF capacitor which makes the low frequency R_{ED} 112 kΩ. This means that high frequency current components are underestimated if V_E is used as a measure of membrane current. Gain, stability, and noise characteristics of the apparatus at our disposal led us to prefer to continue to use the V_E signal for normal voltage clamp work rather than the potentially more faithful I_E signal. Therefore we devised a first-order electronic correction procedure to restore the missing high frequency components in the recorded trace. The signal I_M from Fig. 1 was run into a single adjustable circuit (Fig. 2 B) analogous to that used in the leak and capacity circuit. An overshoot could be added with adjustable amplitude and time constant. The result, shown as the bottom trace in Fig. 6 B, closely resembles the I_E signal from amplifier A3. In each experiment the I_M signal with a square pulse in E was first adjusted to resemble the I_E signal and from then on only the I_M signal was recorded. The setting of the two controls was very similar from fiber to fiber, except in some experiments where we attempted to avoid the problem by covering the entire fiber up to the cut end with Vaseline. This maneuver did eliminate the overshoot but also led to problems of activity under the very long seal. If the apparatus were to be redesigned it might be preferable to aim for using the more faithful I_E signal at all times. This would mean that the absolute size of currents would always be known and would permit the correct current waveform to be used in compensating for the effects of series resistance. This section concludes the analysis of the performance of the method and we turn now to consider electrical properties of the muscle fiber preparations obtained.

Passive Electrical Properties of Muscle Preparations

We were not primarily interested in the passive properties of our preparations but they seemed worth determining both to check that the new method gives reasonable values and to establish an equivalent circuit to use to calculate errors from activity in transverse tubules under voltage clamp. In all over a hundred good muscle preparations were studied at various stages in the evolution of the new method. An equal number were rejected because they were very leaky or because they were destroyed by oscillations of the first amplifier before they could be studied. The passive electrical properties of the preparations using the

Vaseline gap technique are in accord with previous microelectrode studies of frog muscle. Measurements on a group of fibers studied at 5°C are given in Table I. Like the rest of our preparations, these fibers have unusually short sarcomere lengths of roughly 1.6 μm. Where cross sections and surface areas of the fiber were needed, they were calculated by treating the cross section as an ellipse with semiaxes a and b estimated under the dissecting microscope. The resistance R_{ED} was calculated from ratios of V_E to I_E when a voltage step was applied to pool E and measured after the transient phase of I_E. Internal resistivity R_i was then calculated from R_{ED} by the equation

$$R_i = R_{ED} \frac{ab}{(k + 0.5\, l)}, \tag{6}$$

which is derived from the same considerations as Eq. 4. The method assumes that all the current enters at the cut end of the fiber in E and that it leaves through the membrane in the A pool with uniform current density. The values for series resistance in Table I were also calculated from R_{ED} as already described but taking the setting on the R_s dial that was actually used in the voltage clamp study of that fiber.

The specific passive membrane properties of muscle fibers cannot be measured directly. Instead one measures the effective resistance and capacitance of the surface membrane with the distributed transverse tubular system in parallel and uses some additional temporal information to attempt to sort out the contributions of each type of membrane. We fitted an equivalent circuit for the fiber by analysis of the membrane current flowing under voltage clamp in

TABLE I

ELECTRICAL PROPERTIES OF MUSCLE PREPARATIONS AT 5°C

Property	Value	No. of fibers	Experiment series
R_{ED}	131 ± 14 $k\Omega$	19	L + M
R_i	204 ± 20 Ωcm	9	L
R_s/R_{ED}	0.060 ± 0.006	14	L + M
R_s	5.9 ± 1.5 Ωcm^2	6	L
R_{eff}	1.7 ± 0.3 $k\Omega cm^2$	9	L
$C_{initial}$	2.2 ± 0.3 $\mu F/cm^2$	7	L
C_{eff}	11.3 ± 1.2 $\mu F/cm^2$	7	L
τ_{eff}	19.5 ± 2.4 ms	16	L + M
$t_{charging}$	5.2 ± 0.6 ms	16	L + M
$E_{threshold}$	−50.5 ± 0.5 mV	29	S
$E_{AP\ peak}$	59 ± 3 mV	13	S
$E_{reversal}$	64 ± 2 mV	25	S
$I_{Na,max}$	4.7 ± 0.7 mA/cm^2	5	L
$g_{Na,max}$	75 ± 9 $mmho/cm^2$	5	L

Values expressed as mean ± SEM. All fibers with a nominal resting or holding potential of −90 mV and bathed in standard isotonic frog Ringer. The fibers in experiment series S are those studied for ionic selectivity in the following paper (Campbell, 1976) with ends cut in 120 mM CsF. All other fibers were cut in 115 mM CsF + 5 mM NaF. In experiment series L the A pool was deliberately widened to 200–300 μm to improve the accuracy of measuring the membrane area. The A pool had the standard width in series M and S.

response to a step change in membrane potential. The membrane was hyperpolarized by a step V_M of −30 to −50 mV from the holding potential of −90 mV, and the step and capacity transient on return to −90 mV studied. The transient shown in Fig. 7 A and B as the current signal I_M corrected for Z_{ED} has a large initial capacity current lasting less than 20 μs followed by a much slower phase lasting many milliseconds. This signal was integrated by an analog integrator to determine the quantity of charge flowing (Fig. 8 A and B). Integration of the signal I_E was also tried with similar but more noisy results. The method of analyzing the integrated record is shown in Fig. 8 B and is similar to that given by Adrian and Almers (1974). Before the step and later after the capacity transient is over, the integral follows straight lines with slopes differing by V_M/R_{eff}, where R_{eff} is the effective membrane resistance. These lines are drawn and extrapolated back until they cross. The time of crossing precedes the step by a time τ_{eff} that is equal to the product of C_{eff} R_{eff} where E_{eff} is the effective membrane capacitance. At time zero the two extrapolated lines are separated by a vertical distance Q_{eff} equal to the product C_{eff} V_M. Similarly the initial step of the charge record (Fig. 8 A) corresponds to $C_{initial}$ V_M where $C_{initial}$ is the capacity charged in the initial brief transient. Finally we also measured a quantity $t_{charging}$ defined as the time to charge 63% of the slowly charging capacity represented by C_{eff}-$C_{initial}$. Table I gives the values of $C_{initial}$, C_{total}, τ_{eff}, $t_{charging}$, and R_{eff} determined on fibers with mean diameters (calculated as $[2a^2 + 2b^2]^{1/2}$) averaging 167 μm and ranging

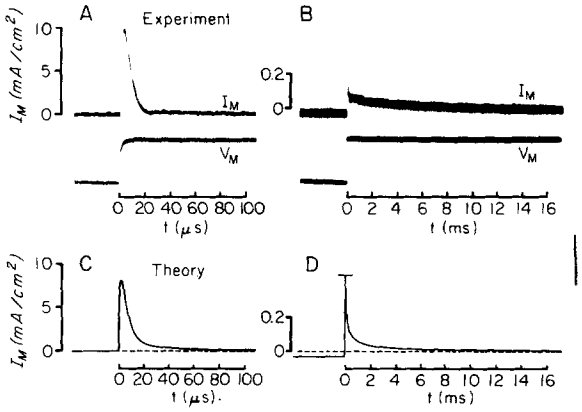

FIGURE 7. Observed and calculated current transients for a potential step from −122.5 to −90 mV. (A, B) Current and voltage records for a fiber cut in 5 mM NaF + 115 mM CsF and bathed in standard Ringer solution. The current in B was filtered by a 10-kHz low pass filter. (C, D) Response calculated from a 150-section disk model integrated in 0.1-μs steps and drawn on the same scales as A and B. In the calculation the membrane potential was assumed to approach its new steady level with a 5-μs exponential time constant. The fit in C would have been better had a time constant of 3.5 μs been used. In addition the calculated current has been drawn as it would appear if recorded by an amplifier with the 2-μs time constant actually measured in a test of our apparatus. The amplified trace in D has been cut off for the drawing. The calculation used the parameter values given in Table II.

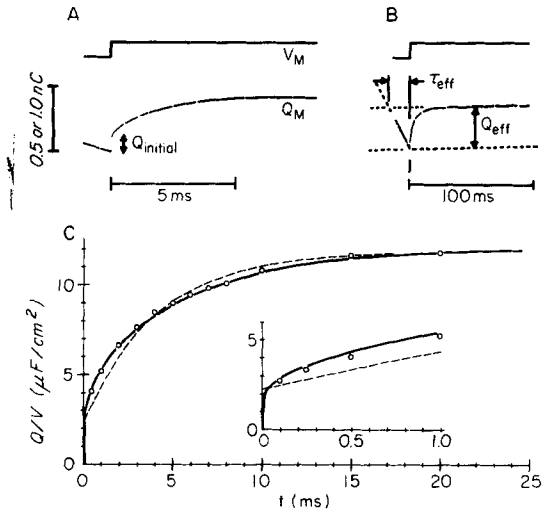

FIGURE 8. Observed and calculated integrated capacity currents during a voltage clamp step from −135 to −90 mV. (A, B) Current integral recorded from a fiber in experiment series L shown at two different sweep speeds and gains. The graphical method for measuring the parameters in Table I is indicated. The area of the fiber was unfortunately not determined so the charge record is not normalized to unit area. The calibration bar is 0.5 nC for A and 1 nC for B. (C) Calculated current integral (smooth curve) from the same simulation as in Fig. 7 C, D but expressed in units of capacity (Q/V). The circles are experimental values read from the records in parts A and B and scaled to give the same value of Q/V at 20 ms. The dashed line is an exponential curve rising from 2.2 μF/cm^2 with a time constant equal to 4.0 ms, which is the same as the calculated $t_{charging}$. The inset shows the early part of the integrated current on an expanded scale. Temperature 5°C.

from 153 to 190 μm. On two smaller fibers of diameters 92 and 125 μm, $C_{initial}$ averaged 1.5 μF/cm^2 and C_{total} was 8.5 μF/cm^2.

The observations on capacity transients were interpreted in terms of a model given by Falk and Fatt (1964) and applied by Adrian et al. (1969), Schneider (1970), and others to the passive electrical properties of the transverse tubular system of muscle. The equations are equivalent to representing the tubular network as a disk extending across the fiber cross section. Following Adrian et al. (1969), the basic constants in the theory are C_W and G_W capacity and conductance per unit area of tubular wall, C_S and G_S capacity and conductance per unit area of fiber surface, and G_L conductivity of the fluid in the tubular lumen. For calculations the tubular constants are converted into practical constants $\tilde{C}_W$ and $\tilde{G}_W$ capacity and conductance of tubules per unit fiber volume and $\tilde{G}_L$ effective radial conductivity of lumen by the geometric factors ρ tubular volume per fiber volume (0.003), ζ volume-to-surface ratio of tubules (10^{-6} cm), and σ the network factor usually set at 0.5.

$$\tilde{C}_W = C_W\rho/\zeta = 3{,}000\ C_W, \tag{7}$$

$$\tilde{G}_W = G_W\rho/\zeta = 3{,}000\ G_W, \tag{8}$$

$$\bar{G}_L = G_L \rho\sigma = 1.5 \times 10^{-3}\, G_L. \quad (9)$$

In order to calculate both passive and active electrical properties from this model, we simulated a patch of fiber surface and the tubular network connected to it on a digital computer as a tapering cable of a finite number of sections following the method of Adrian and Peachey (1973) and using their Eqs. 19-22. The surface membrane was assumed to be isopotential and the potential changes at the surface under voltage clamp were assumed to approach their final value with an exponential time constant of 5 μs. To obtain a fairly correct simulation of the early part of the capacity transient the tubular cable had to be represented by more than the 16 sections used by Adrian and Peachey (1973) for other purposes. We used 150 sections and integrated by the simple Euler method in time steps of 0.1 μs.

Constants can be chosen in the "disk" equivalent circuit to make capacity transients agreeing with the observations. The parameters were chosen by trial and error comparing simulations to observations in the following order. Tubular wall capacity C_W was assumed to be 0.9 μF/cm^2 (Hodgkin and Nakajima, 1972 *b*) and a combination of luminal conductivity G_L and wall conductance G_W was found that gave an appropriate effective tubular capacity and charging time in the simulation. Finally, surface conductance G_S and capacity C_S were added to give appropriate values of R_{eff} and $C_{initial}$. The simulations in Figs. 7 C, D and 8 C, D used the constants given in Table II and a diameter of 167 μm giving the following calculated values: $C_{initial}$ 2.2 μF/cm^2, C_{eff} 11.9 μF/cm^2, R_{eff} 1.7 kΩcm^2, τ_{eff} 20.2 ms, and $t_{charging}$ 4.0 ms. The value determined for $C_{initial}$ includes 0.45 μF/cm^2 from the outermost sections of the tubular cable that charge during the first 25 μs. More than half the fibers studied had values of $t_{charging}$ longer than 4 ms. These longer times could be simulated by decreasing G_L and G_W in parallel, although the value of G_L would then fall well below the range previously encountered in the literature. An alternative approach is to add an external "access resistance" in series with the outermost cable section of the tubules (Adrian and Peachey, 1973). In the extreme this approach returns to the classical two-time constant equivalent circuit of Falk and Fatt (1964) and predicts a single

TABLE II

CONDUCTANCE AND CAPACITANCE IN MUSCLE EQUIVALENT CIRCUIT AT LOW TEMPERATURE

	Hodgkin and Nakajima (1972 *b*)	This paper uncorrected	Correction factor	Corrected for shrinkage
C_S ($\mu F/cm^2$)	0.9	1.75	$\delta^{-1/2}$	1.37
C_W ($\mu F/cm^2$)	0.9	0.9	1	0.9
G_S ($mmho/cm^2$)	0.062	0.410	$\delta^{-1/2}$	0.322
G_W ($mmho/cm^2$)	0.0155	0.0155	1	0.0155
G_L ($mmho/cm$)	3.9	3.12	δ^{-1}	1.9
λ_T (μm)	112.2	100.4	$\delta^{-1/2}$	78.8
$\bar{P}_{Na,S}$ (cm/s)	–	20.0×10^{-4}	$\delta^{-1/2}$	15.7×10^{-4}
$\bar{P}_{Na,W}$ (cm/s)	–	0.2×10^{-4}	1	0.2×10^{-4}

Values from Hodgkin and Nakajima are those given for 3.3-3.9°C except G_S which was scaled from their value at room temperature using their Q_{10} of 1.49. Values from this paper are for 5°C.

exponential charging transient under voltage clamp like the dashed line in Fig. 8 C. Adding access resistance does not improve the fit for the fiber of Fig. 8 but would improve the fit for the fiber of Fig. 7 which was studied at a different time of year. We have done too few experiments to comment on whether access resistance appears systematically in certain types of frogs.

Before the constants labeled "uncorrected" in Table II are compared with values from other preparations, we attempt to take into account the effect of fiber shortening to calculate the constants that would have been found had the fiber remained at normal sarcomere length. We define the sarcomere length ratio δ as the ratio of sarcomere length in the test fiber (1.6 μm) to that in a standard fiber (2.6 μm). If a fiber shortens at constant volume, then the surface membrane will wrinkle and bunch up so that 1 cm^2 of the shortened fiber surface has $\delta^{-1/2}$ cm^2 of the surface membrane material of the reference fiber. Accordingly in the column labeled "corrected for shrinkage" in Table II the fitted values of G_S and C_S have been scaled by $\delta^{-1/2}$. In our fibers a fine wrinkling of the surface was obvious on microscopic inspection. The method for scaling the tubular parameters C_W, G_W, and G_L was suggested to us by Dr. Wolfhard Almers. Both C_W and G_W are unchanged since they are determined from practical constants defined per unit volume (Eqs. 7 and 8), and volume is preserved. However, G_L should change on fiber shortening. How much depends on undetermined geometrical changes of the tubular system as it stretches to span the broader diameter of a shortened fiber. We assume that in addition to the tortuosity implied by the geometric network factor σ, the tubular system of a normal fiber is wavy and slack. When the fiber shortens, the transverse waves of the tubules are assumed simply to straighten without affecting the volume of the tubules or lengthening the total distance that luminal current actually flows in going from, for example, the center of the fiber to the surface. Upon shortening, both the fiber radius and the quantity of surface membrane per surface area increase by $\delta^{-1/2}$, so the effective radial conductivity $\bar{G}_L$ and hence the deduced luminal conductivity G_L increase by δ^{-1}. Using this assumption, the corrected luminal conductivity of 2.0 mmho/cm is 26% of the value calculated for Ringer solution at 5°C. In the remainder of this paper, corrected values of surface and luminal conductances are used. Dependence of electrical parameters on sarcomere length has been reported before (e.g., Valdiosera et al., 1974), but available measurements are not sufficient to test the scaling rules. The geometrical assumptions made above could be tested directly by morphometric measurements.

Action Potentials of Muscle Preparation

Membrane action potentials could be elicited by applying short stimuli to the E pool (Figs. 3 E, 6, and 9 A). In intact muscle, action potentials measured by conventional microelectrode methods last about 10 ms near 5°C, and their repolarizing phase ends fairly abruptly in an appreciable depolarizing afterpotential (Adrian et al., 1970 *a,b*; Hodgkin and Nakajima, 1972 *a,b*). In our preparations cut in CsF the action potentials are usually several times longer with a slow repolarizing phase that merges much more gradually with the afterpoten-

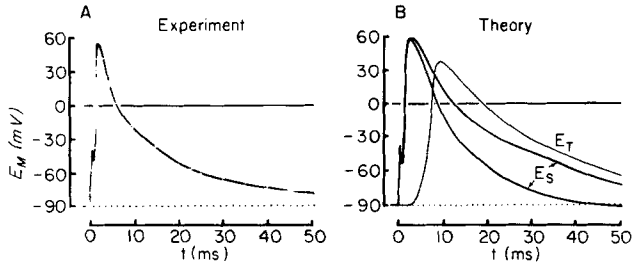

FIGURE 9. Observed and calculated action potentials at 5°C. (A) Action potential elicited by a brief stimulus applied to the E pool. Fiber from experiment series S cut in 120 mM CsF and bathed in standard Ringer solution. (B) Action potentials calculated from a 20-section disk model integrated in 5 μs steps. Traces E_S are the surface membrane potential using standard values (Campbell and Hille, 1976) for the parameters except that for the more quickly repolarizing trace, the surface and tubular membrane leakage conductances were doubled. The trace E_T is the tubular membrane potential in the most central cable section for standard parameters. $\bar{P}_{Na,S} = 14.7 \times 10^{-4}$ cm/s. $\bar{P}_{Na,W} = 0.2 \times 10^{-4}$ cm/s. $E_{Na} = 64$ mV. Stimulus 400 or 440 μA for 0.4 ms.

tial. The shape of the action potential is like that of intact fibers with delayed rectification blocked by external zinc or tetraethylammonium ions (Stanfield, 1973), and indeed, as is shown later, our fibers have lost their delayed rectification. Mean values of the firing threshold potential $E_{threshold}$ and the peak of the action potential E_{peak} are given in Table I for fibers cut in CsF. The threshold potential was measured by applying just-threshold short shocks as in Fig. 3 F and measuring the most negative value of the membrane potential in the period between the shock and the rapid rising phase of the action potential. The mean value −50.5 mV was a few millivolts less negative than reported in intact fibers using long shocks, higher temperatures, and different criteria (Costantin, 1968; Kao and Stanfield, 1968). The peak of the action potential 59 mV was far more positive than in intact muscle because fibers cut in pure CsF have little internal sodium or potassium and little delayed rectification. Fig. 9 B shows a computer simulation of action potentials using the disk model for passive properties and the ionic current model developed in the third paper (Campbell and Hille, 1976). Calculated surface action potentials are given for two values of leakage conductance. The firing thresholds are −53.3 and −51.0 mV and the action potential peaks are 58 and 57 mV. The calculated action potential with the standard leakage conductance in Fig. 9 B falls more slowly than the measured one in Fig. 9 A. Unfortunately we neither have action potential records from the series of fibers used for developing the ionic current model nor from the series used for passive properties. Therefore we are not sure if the difference in action potential duration is important. Fig. 9 B also shows the calculated action potential in the tubular system at the center of the fiber. It reaches a peak of 37 mV. The 5.7-ms conduction delay from surface to center (measured from 0-mV crossing) corresponds to a radial conduction velocity of 1.46 cm/s uncorrected,

and 1.15 cm/s corrected for shrinkage. The measurements of Gonzáles-Serratos (1971) give 2.5 cm/s when adjusted to 5°C.

Ionic Currents under Voltage Clamp

Under voltage clamp with large depolarizing steps, the membrane currents are dominated by currents in sodium channels. Fig. 10 A shows a family of total membrane currents for a fiber depolarized to voltages ranging from −90 to +50 mV in steps of 15 mV. The same steps are repeated in Fig. 10 B but now with the leak and capacity subtractor connected. These currents are carried almost exclusively in sodium channels as defined by sensitivity to block by tetrodotoxin. Fig. 10 C shows the residual currents in 500 nM tetrodotoxin recorded at higher gain with the same 11 voltage steps in another fiber. The fast capacity transient has been prolonged in the picture by a 3-kHz low pass filter at the oscilloscope but otherwise no time-variant currents are seen. The peak of the largest inward sodium current in Fig. 10 B is 4.0 mA/cm^2. Table I gives mean values of 4.7 mA/cm^2 for the maximum inward sodium current and 75 mmho/cm^2 for the peak observed sodium conductance (measured near +40 mV) for a group of fibers bathed in Ringer's solution at 5°C. The mean reversal potential for current in sodium channels was 64 mV for fibers cut in 120 mM CsF and bathed in Ringer. As expected the reversal potential is higher than the 59-mV peak of the action potential in the same group of fibers.

In tetrodotoxin-treated fibers several other tiny currents can be seen. They

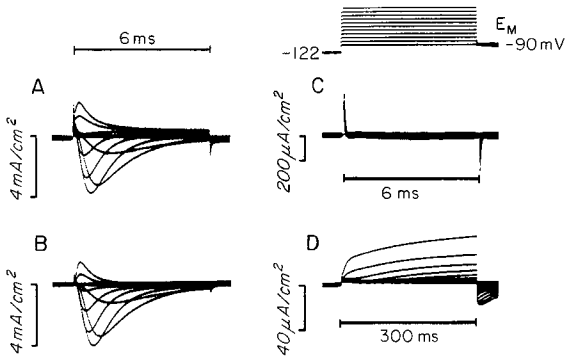

FIGURE 10. Membrane currents recorded from muscle fibers under voltage clamp at 5°C and compensated for series resistance and Z_{ED}. Each frame shows currents for voltage clamp steps to 11 potentials spaced at 16-mV intervals from −90 mV to +70 mV. (A, B) Six-ms depolarizations of a fiber cut in 5 mM NaF + 115 mM CsF and bathed in standard Ringer solution. Same fiber as in the experiment of Fig. 7. The currents were recorded with (A) and without (B) the leak and capacity subtracting circuit. Low pass filter 30 kHz. (C) Six-ms depolarizations of a different fiber treated with 500 nM tetrodotoxin showing block of sodium current. Note higher gain. Low pass filter 3 kHz. (D) 300-ms depolarizations of a third fiber treated with 500 nM tetrodotoxin showing typical tiny delayed outward currents. Low pass filter 1 kHz. Muscle fiber cut in 5 mM 115 mM KF + 5 mM sodium phosphate buffer, pH 7.4.

are so small, however, that their apparent amplitude or time-course can be changed by small adjustments of the leak and capacity circuit, and therefore we have not given them much attention. At high sweep speeds and with large depolarizations a brief transient outward current flows with an amplitude and time-course relative to sodium currents that closely resembles the currents ascribed to sodium channel "gating" in squid giant axons (Armstrong and Bezanilla, 1974; Keynes and Rojas, 1974). In addition, with very long and large depolarizations there are small delayed outward currents (Fig. 10 D) possibly arising in the delayed and the very delayed potassium channels (Adrian et al., 1970 *a,b*). This signal should be reexamined using the more faithful current signal I_E to guard against some slow rectification in the impedance Z_{ED}. The delayed currents were followed by a pronounced inward "tail" current when the membrane was repolarized. The tail current increased when the depolarization was lengthened. To our considerable surprise, the delayed currents were tiny whether the fibers were cut in CsF, or KF, or K_2SO_4, and we were not able to find conditions giving delayed outward currents of the 1-mA/cm^2 size expected from previous work on intact fibers (Adrian et al., 1970 *a,b*). The fiber in Fig. 10 D cut in 115 mM KF + 5 mM NaF did not give more outward currents than that of Fig. 10 C cut in 115 mM CsF + 5 mM NaF.

Although the transverse tubular system of skeletal muscle is known to be electrically excitable (Costantin, 1970; Bastian and Nakajima, 1974), the magnitude of the tubular sodium conductance is not yet known. Fortunately the time-course of the total sodium current observed under voltage clamp offers some clues, if the passive properties of the fiber are known. The contribution of tubular Na channels can be simulated on a computer making the untested assumption that the tubular channels have the same kinetic properties as surface channels and have a uniform density throughout the tubular network different from the surface density. Simulation with the disk equivalent circuit shows that tubular sodium current should stand out most prominantly in voltage clamp steps to near the firing threshold for action potentials, as in the calculated currents in Fig. 11 A. Here the model is stepped from −90 to −50 mV and, to imitate the experimental situation, membrane currents are calculated with leak and capacity currents appropriate to an inexcitable fiber subtracted. Various values of maximum sodium permeability $\bar{P}_{Na}$ are assigned to the tubular membrane. At least for values of $\bar{P}_{Na}$ greater than 0.2×10^{-4} cm/s, the tubular system ultimately fires an action potential that propagates to the middle of the fiber. The extra current drawn by the tubules appears either as a secondary peak or a sharper peak on the calculated total current record. Adrian and Peachey (1973) give similar calculations.

Muscle fibers studied at 12–15°C do show anomalous inward current shapes in the potential range from −70 to −30 mV (Fig. 11 B) with properties like those expected for tubular sodium current. The extra current is blocked by externally applied tetrodotoxin, but only very much more slowly than the major sodium current is. As the extra current is slowly blocked, its time to peak lengthens considerably in a way reminiscent of the simulation in Fig. 11 A. In several experiments with long exposure to tetrodotoxin followed by a rinse in toxin-free

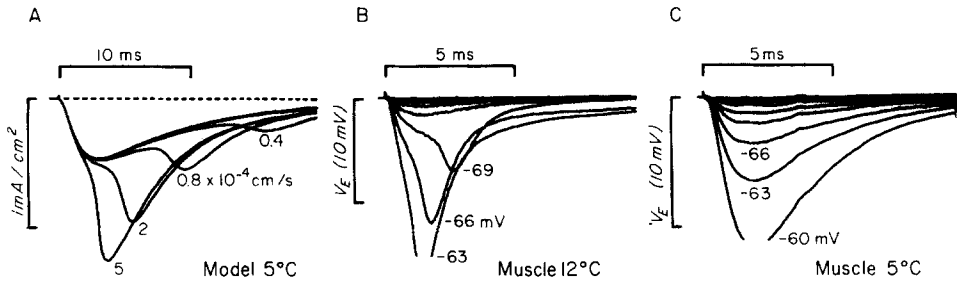

FIGURE 11. Calculated and observed tubular sodium currents superimposed on surface sodium currents. (A) Simulation from the disk equivalent circuit for step depolarizations from −90 mV to −50 mV with $\bar{P}_{Na}$ of the surface 14.7 × 10^{-4} cm/s. $\bar{P}_{Na}$ of the tubules set at 0.1, 0.2, 0.4, 0.8, 2.0, and 5 × 10^{-4} cm/s. E_{Na} = 45 mV. Standard rate constants for 5°C from Campbell and Hille (1976) integrated in 4-μs steps using 20 cable sections. (B) Recorded membrane current (given as V_E) minus leak and capacity for nine voltage clamp steps at 3-mV intervals ranging from −87 to −63 mV. Fiber cut in 5 mM NaF + 115 mM CsF and bathed in Ringer solution at 12°C. The traces at −69, −66, and −63 mV show an extra inward sodium current attributed to tubular excitation. (C) Membrane currents recorded 25 min later from the same fiber cooled to 5°C and depolarized in 10 steps ranging from −87 to −60 mV. The bump in the traces near 4 ms is artifact from a bump in the base-line trace recorded by the computer.

Ringer the extra inward current was no longer evident. Cooling the fiber has a similar effect, delaying the time to peak and decreasing the size of the resolvable extra current, until at 5°C (Figs. 10 B and 11 C) the current is no longer obvious. Nevertheless, by raising the gain, filtering the current record and lengthening the clamp pulse, the extra current can usually be found even in the cold. For example with the fiber of Fig. 10 A,B an 8-μA/cm^2 secondary bump was found at 6 ms with a depolarization to −30 mV. Therefore on the basis of the small size of the extra current we conclude that a reasonable value for $\bar{P}_{Na}$ of the tubular membrane is 0.2 × 10^{-4} cm/s which is 1.3% of $\bar{P}_{Na}$ for the surface membrane. The present estimate is probably inaccurate, but a more systematic study comparing measurement of passive properties and sodium currents with simulations might well be the best available way to determine $\bar{P}_{Na}$ in the tubular membrane.

How much current is attributable to tubular activity with larger depolarizations? Fig. 12 shows a simulation of a complete voltage clamp series with and without tubular Na channels. With a tubular $\bar{P}_{Na}$ of 0.2 × 10^{-4} cm/s and for depolarizations beyond −45 mV, the tubular sodium current is too small relative to the surface current to disturb experimental conclusions concerning amplitudes or time-courses of sodium permeability changes. This might seem surprising since with almost 10 times as much tubular membrane as surface membrane, roughly 12% of the Na channels of the simulated fiber are in tubules. These channels contribute disproportionately little because of the luminal resistance in series with them. The statement can be made more quantitative by converting from permeability to conductance units and using linear cable theory. At 0 mV, chord conductance g_{Na} can be calculated from P_{Na} by

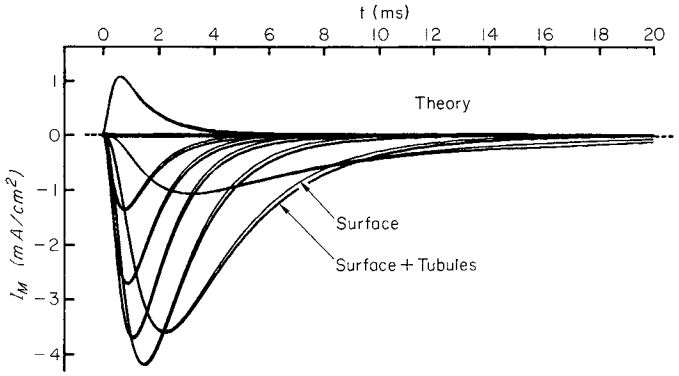

FIGURE 12. Simulation of a complete family of voltage clamp currents for a fiber held at −90 mV and depolarized to eight different levels ranging in 15-mV steps from −45 to +60 mV. Thick lines are the total membrane current minus the leak and capacity currents calculated from the passive circuit without sodium permeability. Thin lines are the sodium current contributed by the surface alone. For all steps from −45 to +45 mV, the excess current contributed by tubules is inward, and even at +60 mV the excess current is inward for the first 10.6 ms. Same integration and parameter values as in Fig. 11 A with $\bar{P}_{Na}$ of tubules set at 0.2×10^{-4} cm/s.

$$g_{Na} = P_{Na}F[Na]_o \frac{e^{(E-E_{Na})F/RT} - 1}{E - E_{Na}}. \quad (10)$$

At 5°C, with $[Na]_o$ = 115 nM and E_{Na} = 45 mV, the entire conversion factor becomes 208.8 mho/cm³ and the assumed $\bar{P}_{Na}$ of the tubules becomes equivalent to a $\bar{g}_{Na}$ of 4.2 mmho/cm². If throughout the tubular system 50% of the channels are active at one moment then there is a total of 21 mmho/cm² of active sodium conductance referred to fiber surface. However, the space constant λ_T of the tubular system, given by $(G_L\sigma\zeta/G_W)^{1/2}$, is then only 6.9 μm and the input conductance of the tubular system, well approximated by $\rho(G_W G_L\sigma/\zeta)^{1/2}$, is only 4.3 mmho/cm². Thus in this case only 21% of the active channels are seen at the surface. Raising P_{Na} in the tubules tends to lower this fraction further, as the input conductance rises only with the square root of the tubular wall conductance.

DISCUSSION

Comparison with Other Methods

This paper is almost exclusively about the development and evaluation of a new voltage clamp method. For certain purposes the new voltage clamp seems to be superior to those previously used on muscle fibers. Compared with the earlier applications of Vaseline gap or sucrose gap potentiometric methods (Frankenhaeuser et al., 1966; Ildefonse and Rougier, 1972; Moore, 1972) our method has more faithful current and voltage records and a procedure for absolute calibration of current density. Compared with microelectrode methods, our method achieves step changes of potential more rapidly, can control the surface mem-

brane even during the rising phase of sodium currents, and allows easy and quick change of external bathing solutions. The method can be applied to a number of questions. We have been able to apply it to studying passive electrical properties and recording ionic currents in Na channels with step changes of potential. The preparation might also be an improvement for sine wave or white noise analysis of equivalent circuits. Because the resolution of our method extends to fairly high frequencies, the question of access resistance to the transverse tubular system would be easier to study. Attempts to sort out the components of conductance contributed by surface and tubular membranes using rapid solution changes would also be easier. It should be possible to look for dielectric currents related to gating or contractile activation by our voltage clamp. Dr. Joe Henry Steinbach working in this laboratory has recorded miniature end-plate currents from fiber fragments with a neuromuscular junction in the A pool. The method is probably not suited to studies of evoked end-plate potentials where an attached conducting nerve fiber is also needed.

On the other hand the new method has some definite disadvantages. The major ones are that fiber fragments shortened by being depolarized and cut may have abnormal electrical properties and that Vaseline gaps are inherently incompatible with mechanical studies. The most obvious electrical abnormality is the absence of delayed rectification in the current record. The delayed rectifier is thought to be somewhat labile in dissected muscle preparations. Whether it is missing in ours because of the period of depolarization, because of the shortening, or because of the presence or absence of a special ingredient in the cutting solution we cannot say at present. A second area of possible abnormality is the geometry of the transverse tubular system. Since the tubules are forced to span a broader fiber cross section in shortened fibers, they may be distorted in unknown ways from their normal morphology. Another disadvantage of the method is that it might be hard to use on small muscle fibers. Finally, as in all gap methods, the exact area of the fiber being studied can be uncertain since the effective position of the insulating Vaseline boundary may be difficult to identify. The fractional error increases as the central pool is made narrower.

Comparison of Fiber Properties

Our measurements of passive properties (Tables I and II) are sufficient to show fair agreement with previous studies. However, our measurements are neither as extensive nor as careful as those of other authors (e.g., Schneider, 1970; Hodgkin and Nakajima, 1972 *a,b*; Valdiosera et al., 1974). We take our values only to indicate that the preparation is fairly normal and that a more careful study of its passive properties could be fruitful. For example, Hodgkin and Nakajima (1972 *a*) found an effective capacity of 8.5–10 μF/cm^2 for semitendinosus fibers of 155–170-μm diameter at room temperature, compared with our 11.3 μF/cm^2 at 5°C. Our 204-Ω cm value for internal resistivity R_i of the fiber is intermediate between the values of 272 Ωcm for intact fibers extrapolated to 5°C (Hodgkin and Nakajima, 1972 *a,b*) and 119 Ωcm calculated from tables in Robinson and Stokes (1965) for 115 mM CsF + 5 mM NaF at 5°C. The compensable 5.9 Ωcm^2 of external series resistance is similar to the 6.4 Ωcm^2 found in squid

giant axons (Hodgkin et al., 1952). The derived surface capacitance C_S is 52% higher and the luminal conductivity G_L, 51% lower in our measurements than in those of Hodgkin and Nakajima (1972 *a,b*). Our fibers consistently have higher peak sodium current densities than reported by other authors using muscle. Adrian et al. (1970 *a*) give figures of 0.6–2 mA/cm² at 2°C and Ildefonse and Roy (1972) give 1 mA/cm² at 20°C. We observe an average value of 4.7 mA/cm², or 3.7 mA/cm² at 5°C after correcting for shrinkage and fit this in our kinetic model (Campbell and Hille, 1976) with a P_{Na} of 15.7 cm/s, equivalent to a limiting $\bar{g}_{Na}$ of 328 mmho/cm² compared with values of 55–70 mmho/cm² found by Adrian et al. 1970 *a*). Almost none of the measurable sodium permeability is attributable to tubular membranes. Our value for P_{Na} in the tubules is equivalent to a limiting conductance $\bar{g}_{Na}$ of 4.2 mmho/cm². Using a Q_{10} of 1.35 this becomes 6.7 mmho/cm² at 20°C, close to the 9.0 mmho/cm² value assumed by Adrian and Peachey (1973). More comparisons with the properties of sodium channels in other excitable cells are given in the following two papers (Campbell, 1976; Campbell and Hille, 1976).

We gratefully acknowledge valuable discussions with Dr. Wolfhard Almers at many points in this work. We thank Susan Morton for invaluable secretarial help, Perry Johnson and Barry Hill for constructing the voltage clamp, and Dr. T. H. Kehl and his staff for providing us with computer facilities.

Supported by grants NS08174, GM00260, NS05082, and FR00374 from the National Institutes of Health.

Received for publication 7 July 1975.

REFERENCES

ADRIAN, R. H., and W. ALMERS. 1974. Membrane capacity measurements of frog skeletal muscle in media of low ion content. *J. Physiol. (Lond.).* **237**:573–605.

ADRIAN, R. H., W. K. CHANDLER, and A. L. HODGKIN. 1969. The kinetics of mechanical activation in frog muscle. *J. Physiol. (Lond.).* **204**:207–230.

ADRIAN, R. H., W. K. CHANDLER, and A. L. HODGKIN. 1970 *a*. Voltage clamp experiments in striated muscle fibres. *J. Physiol. (Lond.).* **208**:607–644.

ADRIAN, R. H., W. K. CHANDLER, and A. L. HODGKIN. 1970 *b*. Slow changes in potassium permeability in skeletal muscle. *J. Physiol. (Lond.).* **208**:645–668.

ADRIAN, R. H., and L. D. PEACHEY. 1973. Reconstruction of the action potential of frog sartorius muscle. *J. Physiol. (Lond.).* **235**:103–131.

ARMSTRONG, C. M., and F. BEZANILLA. 1974. Charge movement associated with the opening and closing of the activation gates of the Na channels. *J. Gen. Physiol.* **63**:533–552.

ARMSTRONG, C. M., and B. HILLE. 1972. The inner quaternary ammonium ion receptor in potassium channels of the node of Ranvier. *J. Gen. Physiol.* **59**:388–400.

BASTIAN, J., and S. NAKAJIMA. 1974. Action potential in the transverse tubules and its role in the activation of skeletal muscle. *J. Physiol. (Lond.).* **63**:257–278.

CAMPBELL, D. T. 1976. Ionic selectivity of the sodium channel of frog skeletal muscle. *J. Gen. Physiol.* **67**:295–307.

CAMPBELL, D. T., and B. HILLE. 1967. Kinetic and pharmacological properties of the sodium channel of frog skeletal muscle. *J. Gen. Physiol.* **67**:309–323.

COSTANTIN, L. L. 1968. The effect of calcium on contraction and conductance thresholds in frog skeletal muscle. *J. Physiol. (Lond.)*, **195:**119–132.

COSTANTIN, L. L. 1970. The role of sodium current in the radial spread of contraction in frog muscle fibers. *J. Gen. Physiol.* **55:**703–715.

DAVIES, P. W. 1974. Voltage clamp measurements on skeletal muscle fibers with low resistance internal electrodes. *Fed. Proc.* **33:**401.

DODGE, F. A., and B. FRANKENHAEUSER. 1958. Membrane currents in isolated frog nerve fibre under voltage clamp conditions. *J. Physiol. (Lond.)*, **143:**76–90.

DODGE, F. A., and B. FRANKENHAEUSER. 1959. Sodium currents in the myelinated nerve fibre of *Xenopus laevis* investigated by the voltage clamp technique. *J. Physiol. (Lond.)*. **148:**188–200.

FALK, G., and P. FATT. 1964. Linear electrical properties of striated muscle fibres observed with intracellular electrodes. *Proc. R. Soc. Lond. B Biol. Sci.* **160:**69–123.

FRANKENHAEUSER, B. 1957. A method for recording resting and action potentials in the isolated frog myelinated nerve fibre. *J. Physiol. (Lond.)*, **135:**550–559.

FRANKENHAEUSER, B., B. D. LINDLEY, and R. S. SMITH. 1966. Potentiometric measurement of membrane action potentials in frog muscle fibres. *J. Physiol. (Lond.)*. **183:**152–166.

GONZÁLES-SERRATOS, H. 1971. Inward spread of activation in vertebrate muscle fibers. *J. Physiol. (Lond.)*. **212:**777–799.

HILLE, B. 1971. The permeability of the sodium channel to organic cations in myelinated nerve. *J. Gen. Physiol.* **58:**599–619.

HODGKIN, A. L., A. F. HUXLEY, and B. KATZ. 1952. Measurement of current-voltage relations in the membrane of the giant axon of *Loligo*. *J. Physiol. (Lond.)*, **116:**424–448.

HODGKIN, A. L., and S. NAKAJIMA. 1972 *a*. The effect of diameter on the electrical constants of frog skeletal muscle fibres. *J. Physiol. (Lond.)*. **221:**105–120.

HODGKIN, A. L., and S. NAKAJIMA. 1972 *b*. Analysis of the membrane capacity in frog muscle. *J. Physiol. (Lond.)*. **221:**121–136.

ILDEFONSE, M., and O. ROUGIER. 1972. Voltage-clamp analysis of the early current in frog skeletal muscle fibre using the double sucrose-gap method. *J. Physiol. (Lond.)*. **222:**373–395.

KAO, C. Y., and P. R. STANFIELD. 1968. Actions of some anions on electrical properties and mechanical threshold of frog twitch muscle. *J. Physiol. (Lond.)*, **198:**291–309.

KEYNES, R. D., and E. ROJAS. 1974. Kinetics and steady state properties of the charged system controlling sodium conductance in the squid giant axon. *J. Physiol. (Lond.)*. **239:**393–434.

MOORE, J. W., F. RAMON, and R. W. JOYNER. 1975 *a*. Axon voltage-clamp simulations. I. Methods and tests. *Biophys. J.*, **15:**11–24.

MOORE, J. W., F. RAMON, and R. W. JOYNER. 1975 *b*. Axon voltage-clamp simulations. II. Double sucrose-gap method. *Biophys. J.*, **15:**25–36.

MOORE, L. E. 1972. Voltage clamp experiments on single muscle fibers of *Rana pipiens*. *J. Gen. Physiol.* **60:**1–19.

NAKAJIMA, S., and J. BASTIAN. 1974. Double sucrose-gap method applied to single muscle fiber of *Xenopus laevis*. *J. Gen. Physiol.* **63:**235–256.

NONNER, W. 1969. A new voltage clamp method for Ranvier nodes. *Pfluegers Arch. Eur. J. Physiol.* **309:**176–192.

RAMON, F., N. ANDERSON, R. W. JOYNER, and J. W. MOORE. 1975. Axon voltage-clamp simulations. IV. A multicellular preparation. *Biophys. J.*, **15:**55–69.

ROBINSON, R. A., and R. H. STOKES. 1965. Electrolyte Solutions. Butterworths & Co. (Publishers) Ltd., London.

SCHNEIDER, M. F. 1970. Linear electrical properties of the transverse tubules and surface membrane of skeletal muscle fibers. *J. Gen. Physiol.* **56**:640–671.

STANFIELD, P. R. 1973. The onset of the effects of zinc and tetraethylammonium ions on action potential duration and twitch amplitude of single muscle fibres. *J. Physiol. (Lond.)*. **235**:639–654.

VALDIOSERA, R., C. CLAUSEN, and R. S. EISENBERG. 1974. Impedance of frog skeletal muscle fibers in various solutions. *J. Gen. Physiol.* **63**:460–491.